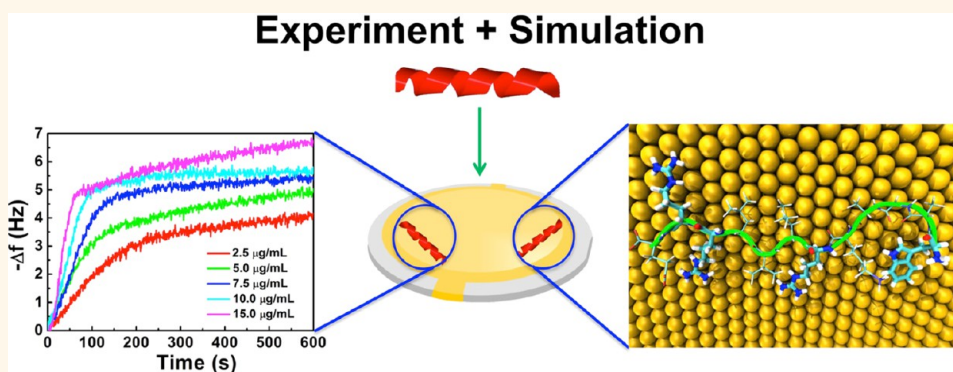


# Biomolecular Recognition Principles for Bionanocombinatorics: An Integrated Approach To Elucidate Enthalpic and Entropic Factors

Zhenghua Tang,<sup>†,‡</sup> J. Pablo Palafox-Hernandez,<sup>‡,§</sup> Wing-Cheung Law,<sup>§</sup> Zak E. Hughes,<sup>‡</sup> Mark T. Swihart,<sup>‡</sup> Paras N. Prasad,<sup>§,¶,\*</sup> Marc R. Knecht,<sup>†,\*</sup> and Tiffany R. Walsh<sup>‡,\*</sup>

<sup>†</sup>Department of Chemistry, University of Miami, 1301 Memorial Drive, Coral Gables, Florida 33146 United States, <sup>‡</sup>Institute for Frontier Materials, Deakin University, Geelong, Victoria 3216, Australia, <sup>§</sup>Department of Chemistry and Institute for Laser Photonics and Biophotonics, and <sup>¶</sup>Department of Chemical and Biological Engineering, University at Buffalo (SUNY), Buffalo, New York 14260, United States, and <sup>||</sup>Department of Chemistry, Korea University, Seoul 151-747, Korea. <sup>#</sup>These authors contributed equally.

## ABSTRACT



Bionanocombinatorics is an emerging field that aims to use combinations of positionally encoded biomolecules and nanostructures to create materials and devices with unique properties or functions. The full potential of this new paradigm could be accessed by exploiting specific noncovalent interactions between diverse palettes of biomolecules and inorganic nanostructures. Advancement of this paradigm requires peptide sequences with desired binding characteristics that can be rationally designed, based upon fundamental, molecular-level understanding of biomolecule–inorganic nanoparticle interactions. Here, we introduce an integrated method for building this understanding using experimental measurements and advanced molecular simulation of the binding of peptide sequences to gold surfaces. From this integrated approach, the importance of entropically driven binding is quantitatively demonstrated, and the first design rules for creating both enthalpically and entropically driven nanomaterial-binding peptide sequences are developed. The approach presented here for gold is now being expanded in our laboratories to a range of inorganic nanomaterials and represents a key step toward establishing a bionanocombinatorics assembly paradigm based on noncovalent peptide–materials recognition.

**KEYWORDS:** bionanocombinatorics · peptides · nanoassembly · simulation · nanoparticles

Established methods are available for synthesizing inorganic nanoparticles of controlled composition, shape, and size;<sup>1–5</sup> however, our ability to assemble these components into a desired 2-D or 3-D pattern lags far behind. Bionanocombinatorics is a new and revolutionary approach that aims to generate predefined complex assemblies of nanomaterials by harnessing molecular recognition, as found

in biology, to control the global and local arrangement of the nanocomponents. Past studies of biomolecule-initiated assembly have mainly relied upon covalent conjugation of proteins or DNA to gold particles.<sup>6,7</sup> Routes to expanding the compositional versatility of such strategies remain uncertain. Employing materials-selective, noncovalent recognition between peptides and inorganic nanomaterials opens up new

\*Address correspondence to pnprasad@buffalo.edu, knecht@miami.edu, tiffany.walsh@deakin.edu.au.

Received for review May 3, 2013 and accepted October 7, 2013.

Published online October 14, 2013  
10.1021/nn404427y

© 2013 American Chemical Society

**TABLE 1. Adsorption Analysis for the Peptide–Gold Interface for All Peptides<sup>a</sup>**

Peptide	Sequence	$\Delta G$ (kJ/mol)	$\theta$ (%)	anchor assignment	entropy assignment
<b>AuBP1</b>	<b>WAGAKRLVLRRE</b>	-37.6 ± 0.9	97.64 ± 0.82	Strong	Medium
<b>GBP1</b>	<b>MHGKTKATSGTIQS</b>	-37.6 ± 1.0	97.70 ± 0.80	Medium	High
<b>B1</b>	<b>LKAHLPPSRLPSP</b>	-36.6 ± 1.2	96.85 ± 1.47	Weak	Medium
<b>AuBP2</b>	<b>WALRRSIRRQSY</b>	-36.4 ± 0.3	95.91 ± 0.45	Strong	Medium
<b>Midas2</b>	<b>TGTSVLIATPYV</b>	-35.7 ± 1.2	95.75 ± 2.00	Weak	High
<b>AgBP2</b>	<b>EQLGVRKELRCV</b>	-35.3 ± 1.2	94.57 ± 2.51	Medium	Medium
<b>Z2</b>	<b>RMRMKMK</b>	-35.0 ± 0.6	92.49 ± 1.07	Medium	Low
<b>QBP1</b>	<b>PPPWLPYMPWPWS</b>	-35.0 ± 1.1	93.61 ± 2.53	Strong	Medium
<b>A3</b>	<b>AYSSGAPPMPPE</b>	-31.8 ± 0.3	82.83 ± 1.26	Strong	High
<b>AgBP1</b>	<b>TGIKSARAMRN</b>	-31.6 ± 0.2	79.83 ± 1.56	Strong	High
<b>Z1</b>	<b>KHKHWHW</b>	-31.3 ± 0.1	81.41 ± 4.54	Medium	Low
<b>Pd4</b>	<b>TSNAVHPTLRL</b>	-30.3 ± 0.2	70.20 ± 0.49	Weak	High

<sup>a</sup> From QCM experiments: adsorption free energies ( $\Delta G$ ) and surface coverage at the highest peptide concentration studied ( $\theta$  at 15  $\mu$ M peptide). Values are given as mean ± one standard deviation from three independent experiments. From molecular simulations: estimated enthalpic component (anchor assignment) and estimated entropic component (entropy assignment). Surface contact residues, determined from molecular simulation for each sequence, are highlighted in green.

possibilities for assembling many combinations of nanoparticles of diverse inorganic materials. However, realizing the full potential of peptide-based bionano-combinatorics requires a fundamental, molecular-level understanding of peptide/nanosurface interactions. Here, we focus on building such fundamental understanding using coordinated large-scale advanced molecular simulation and experimental binding measurements, with gold-binding as a prototypical example.

Numerous gold-binding peptide sequences have been identified,<sup>8–16</sup> as summarized in Table 1; several of these sequences have been employed for the fabrication of ligand-capped nanoparticles.<sup>10,17</sup> The few that have been rigorously characterized, including the 3R-GBP1 (triple repeat of the GBP1 sequence),<sup>18</sup> AuBP1, and AuBP2<sup>8</sup> peptides, showed binding affinities similar to those of thiols on gold. The fact that gold-binding peptides have been previously isolated and examined under varying conditions hinders intercomparison of the results from these different studies on an equal footing. Similarly, molecular simulation has been applied to several gold-binding peptides,<sup>19–23</sup> but the varying conditions and methods employed previously again makes intercomparison problematic. Further, materials-binding peptides are challenging to model, due to the wide range of conformations they can assume.<sup>24</sup> Because almost all of these previous modeling studies employed standard molecular dynamics (MD) or Monte Carlo simulations that take no special measures to ensure thorough and robust sampling of conformational space, the structures reported may not be representative, compromising the conclusions that can be drawn.

Here we present a systematic study of peptide binding on gold, where we have quantitatively measured the kinetics and thermodynamics of binding for the 12 sequences in Table 1. Such measurements were

performed under identical conditions, thus allowing for direct intercomparison of the experimental results. We have also employed our newly developed MD simulation protocol, applying Replica Exchange with Solvent Tempering (REST)<sup>25</sup> sampling for biointerfaces, combined with our recently developed interaction potentials for this system.<sup>26</sup> REST is a novel, computationally efficient, Hamiltonian-based replica-exchange approach; it enables conformational sampling that is comparable with conventional (temperature-based) replica-exchange methods, but at a fraction of the required computing resource. In very recent work we have developed and verified adaptations of REST specifically tailored for peptide-materials interfaces.<sup>24</sup> Our simulations of the peptide–gold interface described herein represent the first application of our biointerface REST approach to investigate peptide–materials affinity. Our simulation results generate a rigorous ensemble of likely bound-peptide configurations, thus allowing us to interpret the experimental findings from a molecular-level perspective. Our combined studies quantitatively show, for the first time, the importance of entropic differences in determining the overall binding affinity. Previously advanced hypotheses regarding peptide–nanomaterials recognition maintained a focus on binding enthalpy considerations, such as the probable number, distribution, and type of residue–nanosurface contacts.<sup>20,22,24,27–32</sup> Some of these simulation studies included consideration of entropic factors: Maranas and co-workers explored the influence of peptide flexibility on peptide binding;<sup>22</sup> Heinz *et al.*<sup>19</sup> estimated configurational (*i.e.*, whole system) entropic changes based on an estimate of the possible reduction of peptide rotameric degrees of freedom combined with the approximate entropy associated with interfacial water release; and in very recent work, Corni *et al.*<sup>32</sup> calculated configurational

entropy change estimates directly from simulation data. However, previous studies, with the exception of Corni *et al.*, did not quantify these entropic considerations on the basis of genuine advanced conformational sampling techniques (*i.e.*, those that are not standard MD approaches). Our previous modeling of materials-binding peptides suggests that strong binding affinity can arise not only from strong peptide–surface interaction energies, but also from the system possessing many different adsorbed conformations.<sup>24,31</sup> The number of adsorbed conformations can provide an estimate of the conformational entropic contribution to the binding. Here, we define conformational entropy to be the entropy associated with the peptide alone, specifically the entropy associated with the number of distinct conformational states (or basins on the energy landscape<sup>33</sup>) that are accessible to the surface-bound peptide. While we recognize that in a majority of instances a peptide will lose entropy upon adsorption to a surface, we postulate that different sequences lose different amounts of entropy, and thus, entropic factors play a role in the resulting binding affinity. We note that experimentally selected materials-binding peptides are typically random-coil in structure and do not usually feature a well-defined, single, native conformation (basin). The links between peptide sequence, structural features, and the enthalpic and entropic factors identified here could be incorporated into advanced informatics approaches to enable the design of materials-binding peptide sequences with predictable binding behaviors. We also show that sequences experimentally selected for strong binding to one material can also be strong binders of other, very different materials. Thus, our comprehensive overview provides a necessary platform for future investigation of the molecular basis of compositionally selective peptide–nanomaterials binding.

## RESULTS AND DISCUSSION

The materials-binding peptide sequences, sourced from previous literature (Table 1), were synthesized as detailed in the Materials and Methods section. This set of peptides includes sequences that were not specifically selected for their ability to bind to gold: two silver binding peptides, AgBP1 and AgBP2,<sup>34</sup> a quartz-binding peptide, QBP1,<sup>35</sup> and a palladium-binding peptide, Pd4.<sup>36</sup> Full details of the provenance of each sequence and the type of target material (*e.g.*, foil, particle, powder) against which it was identified are given in Table S1 of the Supporting Information, where complete literature citations are also included.

The binding affinity of a particular sequence is characterized by the difference in Gibbs free energy between the bound and unbound states,  $\Delta G = \Delta H - T\Delta S$ , which is related to the equilibrium constant for binding ( $K_{eq} = \exp(-\Delta G/RT)$ ). We can associate  $\Delta H$  with the number and strength of anchor residue contacts,

defined as those with strong and persistent affinity for the surface. On the other hand,  $\Delta S$  depends upon the conformational freedom of the peptide adsorbed on the inorganic surface. The Gibbs free energy is experimentally accessible through measurements of the binding equilibrium,<sup>37,38</sup> for which we employed Quartz Crystal Microbalance (QCM) techniques, as detailed in Materials and Methods. These measurements provide a measure not only of the amount of peptide bound, but also of the dissipation energy associated with the layer of bound peptide. The latter provides information about the rigidity of the bound layer. Analysis of molecular simulation results in light of the experimental results allowed us to compare enthalpic and entropic effects and relate them to molecular features.

**QCM Analysis of Peptide Binding.** QCM has been employed to quantitatively measure the adsorption of biomolecules on target interfaces, including inorganic surfaces.<sup>18,39,40</sup> To measure peptide adsorption, gold coated sensors were used. Note that the metallic gold surface is polycrystalline; thus, a distribution of gold crystal orientations and facets is presented to the solution. Initially water was flowed over the sensor surface to establish a baseline, followed by flowing the aqueous peptide solution at known concentrations. Figure 1 presents the QCM analysis for two of the peptides studied here. Figure 1a specifically presents the analysis for the AuBP1 peptide isolated by Sarikaya and colleagues.<sup>12</sup> When a peptide concentration of 2.5  $\mu\text{g/mL}$  was flowed over the gold surface, a decrease in the resonant frequency was observed that saturated at a value of  $-4.0\text{ Hz}$ . This corresponds to approximately 100 ng of adsorbed peptide per  $\text{cm}^2$  of gold surface, based on the superficial area of the QCM chip, not accounting for additional surface area due to roughness. Note that inverted plots are displayed for more intuitive data presentation. Higher peptide concentrations produced larger and faster frequency shifts, reflecting increased binding rates and increased totals of peptide bound at saturation. At all peptide concentrations, negligible dissipation energy associated with the elasticity of the bound peptide layer was observed at <5% of the total frequency change. This is shown by the purple plot in Figure 1a for the 15  $\mu\text{g/mL}$  analysis. As is evident there, no energy dissipation was observed in this experiment. This indicates that the adsorbed layers were quite rigid, and suggests that only a single peptide layer is adsorbed on the gold surface. If a multilayer structure was formed, greater surface elasticity would undoubtedly be present, resulting in a measurable dissipation energy. Similar results were obtained for all the peptides studied; negligible dissipation energy was recorded in all cases for the concentration range used in this study. Results for the Pd4 peptide (Figure 1b), originally isolated for Pd binding,<sup>36</sup> show that it also bound appreciably to the gold surface,

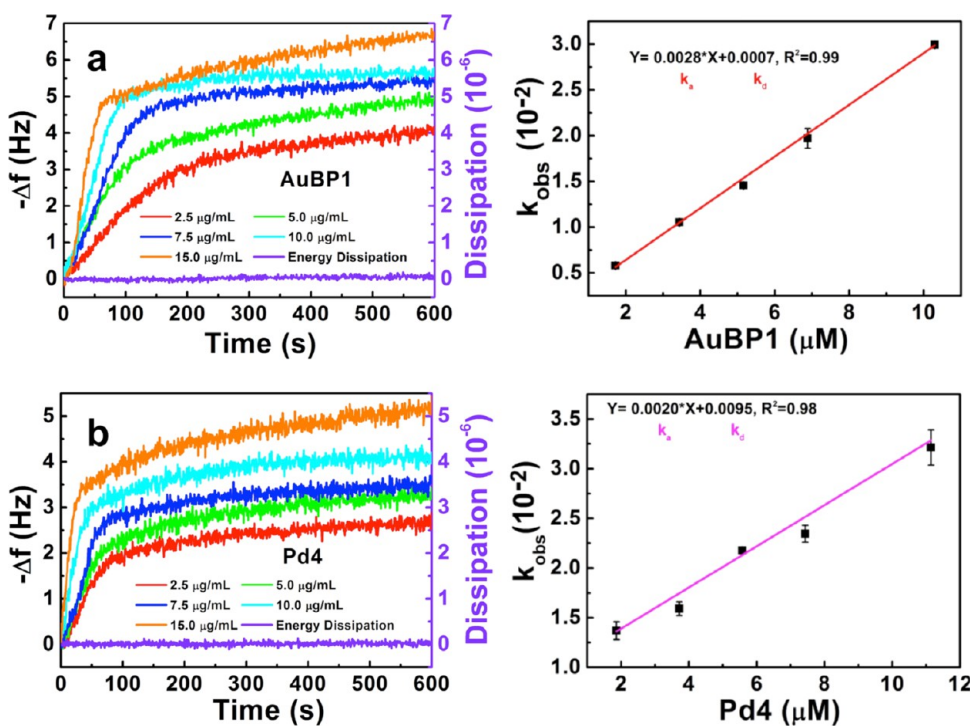


**Figure 1.** QCM analysis of peptides (a) AuBP1 (strongest binder) and (b) Pd4 (weakest binder) to obtain  $k_a$  and  $k_d$  values. Left panels show inverted frequency change vs time, for five concentrations of each peptide, as well as the dissipation energy plot for the highest concentration studied. Right panels show plots of  $k_{obs}$  values vs peptide concentration, obtained from the data in the left panels by fitting to Langmuir kinetics. The slopes of the plots in the right panels give the adsorption rate constants, while the y-intercepts provide the desorption rate constants.

although it ultimately proved to be the weakest binder among the peptides in Table 1. Again, no measurable dissipation energy was observed, as indicated by the purple plot for the 15  $\mu g/mL$  Pd4 sample during the binding analysis.

While it is clear that peptide binding to the gold surface occurs, it must be noted that it is challenging to experimentally determine the molecular-scale structure of this interface. This is especially true for the polycrystalline gold QCM sensor, where the surface roughness prevents direct imaging of the biological layer. Previous studies have attempted to image gold-bound peptides on a single crystal Au(111) surface using atomic force microscopy (AFM), which indicated the formation of surface peptide patterns; however, these adsorbed layers were dried prior to analysis.<sup>18,41,42</sup> Unfortunately, drying is likely to dramatically alter the surface structure, both because of the capillary forces that act on the layer during drying and because the ordered water layers adjacent to the gold surface and the water molecules associated with the peptide play important roles in peptide binding. Thus, these images may not be reflective of the bound peptide morphology of the materials in water. Interestingly, for all of these studies, the biological layer thickness corresponded quite well with values for the anticipated thickness of a peptide monolayer on the gold surface, suggesting that multilayer formation was not occurring.<sup>18,41,42</sup> Furthermore, in the study by

Singamaneni and co-workers, single, monolayer coverage of the A3 peptide binding to the Au(111) surface was observed at concentrations up to 20  $\mu g/mL$ .<sup>41</sup> Below this concentration, single peptide layers were noted; however, they were observed to not fully coat the gold surface. For our study, the concentrations for all of the peptides, including the A3 sequence, are studied at <20  $\mu g/mL$ , consistent with the formation of a single peptide layer at the metallic interface.

Our QCM results strongly suggest that a peptide monolayer forms on the sensor surface under these experimental conditions. We do not see any evidence for build-up of multiple layers of peptide (multilayers). Furthermore, previous studies using single crystal gold surfaces,<sup>18,41,42</sup> have shown that this layer generates a patterned surface, thus forming less dense layers as compared to standard alkyl thiols on gold.<sup>43</sup> Monolayer formation of this type is indicated by the lack of energy dissipation as discussed earlier, which demonstrates that a rigid layer is bound to the gold sensor. Should a multilayer structure be formed, the loosely bound peptides in the outer layers would interact significantly with the solvent, producing a viscoelastic layer with significant and measurable dissipation energy. Because the peptide interface is rigid, the layer thickness can be roughly estimated by eq 1:<sup>44</sup>

$$d = \frac{\Delta m}{\rho} \quad (1)$$

Here,  $d$  represents the film thickness,  $\Delta m$  is the mass of peptide bound to the QCM sensor surface, and  $\rho$  is the effective density of the adhering layer. The peptide density can be approximated using previous methods,<sup>45</sup> however, this assumes formation of a complete layer of peptide with no defects or patterning. Using these values, the thickness of the peptide layer at the lowest and highest peptide concentration studied was examined, and the film thickness for all of the experiments performed here was  $\leq 8.9$  Å, as shown in the Supporting Information, Table S2. Should the peptides lay completely flat on the gold, with all residues interacting with the surface, a typical film thickness of 4 Å would be expected, simply based on the geometry of the molecules. Such a binding event is unlikely, due to peptide steric constraints and interactions with the solvent, thus a higher value closer to the ones calculated for our experiments is likely. Taken together, this evidence indicates that peptide monolayers are formed on the gold sensor surface under the conditions used in this study. Monolayer formation is further supported by the kinetic and equilibrium analysis presented below.

Each QCM-derived binding curve was fit using Langmuir kinetics, from which  $k_{\text{obs}}$  values for each concentration were determined using previously described methods.<sup>18,46</sup> Plotting the  $k_{\text{obs}}$  values as a function of the AuBP1 peptide concentration, as in the right panel of Figure 1a, gives the rate constants for adsorption ( $k_a$ ) and desorption ( $k_d$ ) as the slope and  $y$ -intercept of the plot, respectively. Note that this approach assumes the formation of a single peptide layer on the Au sensor surface. If multilayer adsorption occurred, based upon peptide–peptide interactions that differ in strength from the peptide–surface interactions, the Langmuir isotherm would not fit the data, nor would a linear trend be observed for the  $k_{\text{obs}}$  values as a function of concentration. The facts that (1) the data were well fit by the Langmuir isotherm, (2) the values of  $k_{\text{obs}}$  increased linearly with concentration, and (3) negligible dissipation energy was measured by QCM suggested that a single peptide layer was generated at the sensor surface. Thus, fitting to Langmuir adsorption kinetics is appropriate. This approach also has the advantage of being consistent with previous studies.<sup>8,12,18,34,46–49</sup> The binding equilibrium constant,  $K_{\text{eq}}$ , can then be calculated as  $k_a/k_d$ . A full summary of the  $k_a$ ,  $k_d$ , and  $K_{\text{eq}}$  values for each peptide can be found in the Supporting Information, Table S3. Note that these values are extracted from the QCM analysis, where multiple peptides are bound to the same sensor surface and not for a single peptide binding to the surface. Upon the basis of the strong evidence of monolayer formation with coverage-independent binding energetics, we believe that the binding kinetics and equilibrium are dominated by peptide–surface interactions; however, a contribution

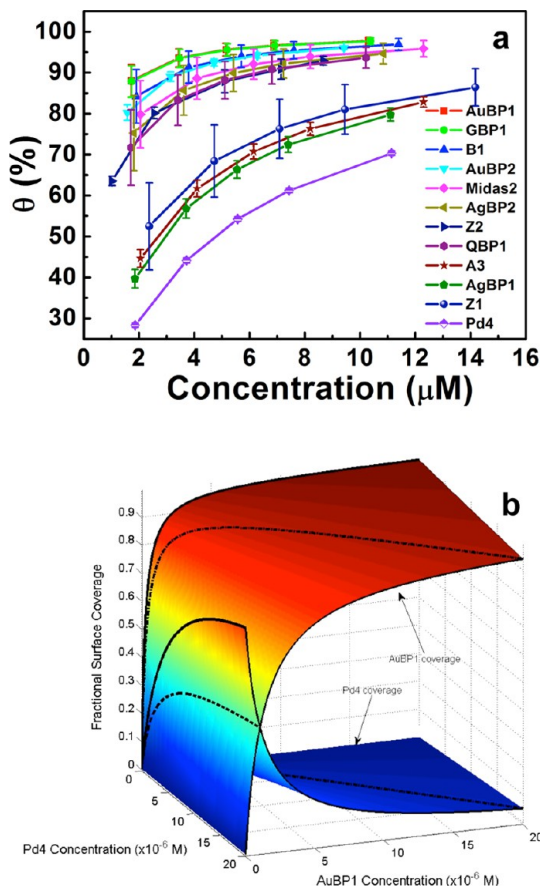
from peptide–peptide interactions in the single layer is inherently included in these values. At present, separating out the effects of peptide–peptide interactions in our measurements is not feasible. However, Wei and Latour, using SPR spectroscopy of septamer peptides adsorbed on SAM surfaces, have quantified the contributions of interpeptide interactions to the peptide-SAM adsorption free energy.<sup>37</sup> They found that the correction in the strong-binding regime amounted to  $\sim 6$  kJ/mol and was consistently of the same sign, meaning that the trend in binding free energies was the same for the corrected and uncorrected data. For the AuBP1 peptide, a  $k_a$  value of  $(2.80 \pm 0.02) \times 10^3 \text{ M}^{-1} \text{ s}^{-1}$  and a  $k_d$  value of  $(7.0 \pm 0.03) \times 10^{-4} \text{ s}^{-1}$  were determined, from which an equilibrium constant of  $K_{\text{eq}} = (4.00 \pm 1.43) \times 10^6 \text{ M}^{-1}$  was calculated. The change in Gibbs free energy for peptide binding,  $\Delta G = -RT \ln(K_{\text{eq}})$ , was  $-37.6 \pm 0.9$  kJ/mol. These values are consistent with a peptide sequence that strongly binds the target surface and are comparable to the binding energies of thiols on Au.<sup>12</sup> For comparison, SPR analysis of the Au binding of AuBP1 was also carried out to confirm the QCM results. From the SPR studies, a  $K_{\text{eq}}$  value of  $(3.82 \pm 0.06) \times 10^6 \text{ M}^{-1}$  was determined, corresponding to a  $\Delta G$  value of  $-37.5 \pm 0.05$  kJ/mol. These results were consistent with the QCM studies and confirmed the strong Au surface affinity of the peptide.

Figure 1b presents results of the same QCM analysis for the Pd4 peptide. For Pd4, a  $k_a$  of  $(2.01 \pm 0.10) \times 10^3 \text{ M}^{-1} \text{ s}^{-1}$  and a  $k_d$  of  $(0.95 \pm 0.04) \times 10^{-2} \text{ s}^{-1}$  were determined. Using these, the  $K_{\text{eq}}$  and  $\Delta G$  values were calculated to be  $(2.11 \pm 0.13) \times 10^5 \text{ M}^{-1}$  and  $-30.3 \pm 0.2$  kJ/mol, respectively. These values demonstrate that the sequence, which was isolated based upon affinity for palladium,<sup>36</sup> does indeed bind to gold surfaces, but binds less strongly than AuBP1, which was isolated specifically for gold binding. This suggests that while peptide affinity for a target can be achieved through the bioselection process, a high degree of specificity cannot be guaranteed based solely on the fact that a sequence was isolated for binding to a particular surface.

The same analysis was carried out under identical conditions for all of the peptides in Table 1, where they are listed in order of decreasing  $\Delta G$  values, ranging from  $-30.3$  to  $-37.6$  kJ/mol for the weakest (Pd4) and strongest (AuBP1 and GBP1) binders, respectively. Interestingly, a bimodal distribution in binding affinities was observed, with a gap in  $\Delta G$  values between the A3 ( $-31.8 \pm 0.3$  kJ/mol) and QBP1 ( $-35.0 \pm 1.1$  kJ/mol) peptides. Sequences isolated or designed for binding to gold were not necessarily stronger binders than peptides isolated for binding to other materials. For instance, AgBP2 was identified by bioselection experiments for binding to silver;<sup>50</sup> however, it possessed a significant affinity for gold ( $-35.3 \pm 1.2$  kJ/mol), higher than that of some sequences specifically selected for

gold affinity. This suggests that promiscuous surface binding may be possible on materials of similar structures. The Z2 peptide, previously described by Belcher and co-workers,<sup>51</sup> was designed as an interdigitated sequence comprised of known binding residues (methionine, arginine, and lysine); however, the affinity of this designed sequence was lower than several of the selected sequences, indicating that the affinity for the target surface requires more than just incorporating a collection of strong binding moieties into the sequence. Additional factors related to the peptide conformation are likely to play a major role in the surface binding capabilities of the sequences.

The Langmuir kinetics fitting of the data also provides a steady-state fractional surface coverage,  $\theta$ , of the sensor for each peptide, as a function of the peptide concentration, as shown in Figure 2a. For the AuBP1 peptide, the surface coverage increased from  $88 \pm 4.0\%$  to  $98 \pm 0.8\%$  as the peptide concentration



**Figure 2.** Fractional surface coverages of peptides. (a) Individual fractional coverages as a function of peptide concentration obtained via QCM in experiments using each peptide separately. (b) Surface coverages predicted for competitive binding of the AuBP1 and Pd4 peptides as a function of concentration in solution, using eqs 1 and 2 in the text. The dashed line indicates where the two surfaces cross, the locus of points where the surface coverages of the two peptides are equal. The dash-dot lines indicate the coverages for equal solution-phase concentrations of the two peptides.

was increased from 2.5 to 15.0  $\mu\text{g}/\text{mL}$ . For the Pd4 peptide, the surface coverage reached a maximum value of  $70.3 \pm 0.5\%$ , consistent with its weaker binding affinity. The surface coverage for the other peptides studied correlated well with the Au affinity. The measured binding equilibrium constants allowed for prediction of the coverages that should prevail if the surface was simultaneously exposed to both peptides at select concentrations, which cannot be directly measured using QCM. The Langmuir adsorption isotherm for competitive binding on the same sites can be written as follows:

$$\theta_{\text{AuBP1}} = \frac{K_{\text{AuBP1}}[\text{AuBP1}]}{1 + K_{\text{AuBP1}}[\text{AuBP1}] + K_{\text{Pd4}}[\text{Pd4}]} \quad (2)$$

$$\theta_{\text{Pd4}} = \frac{K_{\text{Pd4}}[\text{Pd4}]}{1 + K_{\text{AuBP1}}[\text{AuBP1}] + K_{\text{Pd4}}[\text{Pd4}]} \quad (3)$$

For equal concentrations of the two peptides, the ratio of the fractional coverages ( $\theta_{\text{AuBP1}}/\theta_{\text{Pd4}}$ ) is simply equal to the ratio of the equilibrium constants ( $K_{\text{AuBP1}}/K_{\text{Pd4}}$ ), which in this case is  $\sim 19.0$ . This is much greater than the ratio of the surface coverages for independent binding of the two peptides (*i.e.*, the coverages in Figure 2a), showing that substantial selectivity of the surface for one peptide over another is possible even when both peptides have significant affinity for the target. Figure 2b presents the fractional coverages of these two peptides predicted by Langmuir competitive binding eqs 2 and 3, as a function of the peptide concentrations in solution. This shows more clearly that, except at very low concentrations of AuBP1, the surface would primarily be covered with AuBP1 and would have very little Pd4. Importantly, this confirms that the differences in binding affinity of a few kJ/mol that are observed here are sufficient to confer substantial selectivity when the peptides are competing for the same surface.

**Molecular Dynamics Simulations of Adsorbed Peptide Structure.** REST<sup>24,25</sup> MD simulations of each aqueous gold–peptide interface were carried out to determine the Boltzmann-weighted ensemble of adsorbed peptide conformations for each sequence. In very recent previous work, we have developed and verified adaptations for REST specifically tailored for peptide–materials interfaces.<sup>24</sup> In our simulations, we consider the binding arising from a single peptide chain adsorbing on the gold surface. We do not calculate binding free energies, however. The meaningful estimation of a genuine adsorption free energy for peptide adsorption at the aqueous interface, derived from atomistic simulation, is currently a daunting task. Such results have not yet been reported for a dodecamer peptide. These adsorption free energies have been reported only recently, and for smaller sequences (5–9 residues).<sup>52–55</sup> In an alternative approach, as detailed in refs 19, 21, and 55, the change in free energy was

estimated as a change in potential energy,  $\Delta PE_{ads}$ , and was calculated *via* a compartmentalized method. In this approach, the Boltzmann weighting of the adsorbed states was not accounted for (the four lowest binding energies<sup>19,21,56</sup> are *linearly averaged*, the fifth lowest data point is discarded), and the accompanying change in entropy was estimated to be constant between different adsorbates. To compare the compartmentalized approach with a genuine free energy-based method, we contrast the binding energies for a range of amino acids (see Supporting Information Section 'Adsorption Energy Comparisons'). Our results show a variable degree of agreement, with large differences between  $\Delta PE_{ads}$  and the adsorption free energy in some cases. Furthermore, the compartmentalized method is predicated on an energetic analysis that is based on limited conformational sampling (derived from multi-initial-configuration standard MD simulations) that does not reflect a Boltzmann-weighted ensemble of conformations (see Supporting Information Section 'Comparison of Sampling Approaches' for details). Moreover, we recognize the potential importance of multichain adsorption, and the concomitant co-operative effects that may arise from the presence of interpeptide interactions, as well as peptide–surface interactions; however, at present, the huge challenges in obtaining adequate conformational sampling relating to adsorption of a single chain,<sup>24,52,53</sup> let alone multichain adsorbed states, makes an unambiguous investigation of these multichain states beyond the reach of current computational methods. There are similar challenges faced in unambiguously resolving questions of single-chain *vs* multichain adsorption *via* experiment. Our results, while presented for the single-chain adsorption scenario, provide a platform for future developments in addressing these grand challenges.

Force-fields developed for describing the interactions of biomolecules with noble metal surfaces include INTERFACE FF<sup>57</sup> and CHARMM-METAL.<sup>58</sup> These force-fields have the advantage of simplicity, being based purely on unmodified Lennard-Jones (LJ) interactions between adsorbate and surface, generated *via* standard combining rules. However, this unmodified LJ form of the force-field always guarantees, by construction, preferential adsorption onto hollow sites on the surface,<sup>59</sup> at variance with current theoretical and experimental conclusions that indicate atop site adsorption is preferred in general (see Chen *et al.*<sup>60</sup> and references therein), even for more complex molecules,<sup>61</sup> and also at the interface with liquid water.<sup>62</sup> The proposed "soft epitaxy" mechanism (see *e.g.*, ref 19), with particular reference to binding selectivity over the (111) and (100) facets, advanced on the basis of simulations employing the CHARMM-METAL force field (and variants thereof), could conceivably be a consequence of the force-field used; very recent work

using the GoLP-CHARMM force-field (*vide infra*) indicates an alternative explanation for this phenomenon.<sup>63</sup> Here, we employ our recently developed polarizable force-field for the interface between aqueous peptides and gold, GoLP-CHARMM.<sup>26</sup> GoLP-CHARMM uses virtual interaction sites to ensure noncovalent adsorption proceeds correctly *via* atop sites. Validation of biointerfacial force-fields for gold at present is challenging and open to extensive interpretation. Few experimental data on adsorption of single amino acids under aqueous conditions are available. While a number of peptide adsorption studies are available (*e.g.*, Willet *et al.*,<sup>64</sup> Hnilova *et al.*,<sup>12</sup> and Cohavi *et al.*<sup>49</sup>), inference of residue-specific binding information is difficult due to the interplay of sequence, conformation, and surface binding. In light of these limitations, both CHARMM-METAL and GoLP-CHARMM are seen to perform reasonably in terms of recovering the trend in the adsorption energies of amino acids. Compared against the more direct observations of Phe adsorption at the aqueous gold interface, reported as  $-18 < \Delta G^0 < -37$  kJ/mol,<sup>65</sup> the GoLP force-fields show good agreement with binding energy. Using metadynamics simulations,<sup>66</sup> we have calculated the genuine free energy of Phe adsorption at the aqueous Au(111) interface to be  $-20.6 \pm 0.5$  kJ/mol using GoLP-CHARMM (see Supporting Information section 'Adsorption Energy Comparisons' for details). While both GoLP-CHARMM and CHARMM-METAL appear to recover the broad features of spatial structuring of interfacial water at the aqueous Au(111) interface, details of the description of the orientational ordering in these interfacial layers for comparison against recent, dispersion-corrected first-principles simulations<sup>67</sup> has to date only been reported for GoLP-CHARMM,<sup>26</sup> which shows very good agreement. The orientational preference of the interfacial water layers could influence the adsorption of the peptide, because this orientation may control the availability of interfacial water for hydrogen bonding. For comparison, we report the same orientational analysis of the interfacial waters for simulations of the aqueous Au(111) interface using CHARMM-METAL, see the Supporting Information 'Aqueous Interface Comparisons' for details. Our orientational data for CHARMM-METAL show an opposite behavior to that reported in refs 26 and 65.

The structural predictions arising from our simulations can be combined with the experimental results above to elucidate the molecular basis for the differing degrees of binding affinity. For all sequences that are not discussed in depth (*vide infra*), we show snapshots of each typical adsorbed conformation in the Supporting Information (Figures S2–S10). For each ensemble, we identified the residues that made the closest and most persistent surface contact (see Materials and Methods). The resulting contact residues are highlighted for each peptide in Table 1. In addition, from

the total set of sequences, we determined the frequency of occurrence for each of the 20 residues (Supporting Information, Table S4); these data show that Ala, Ser, Thr, Leu, Pro, Lys, and Arg are the most abundant residues in our set of 12 peptides. We then calculated the relative fraction of each of these residues that is present in our set of contact residues (Supporting Information, Table S5). Other than Arg, the set of the most abundant contact residues does not overlap with the set of most abundantly occurring residues, demonstrating that our set of contact residues did not arise merely as a consequence of their abundance. The most frequently occurring contact residues, Met, Trp, Phe, His, Tyr, and Arg, which we designate as anchor residues, have been previously reported to be the most strongly binding of all naturally occurring amino acids at the aqueous Au(111) interface;<sup>26,56,68</sup> however, these previous calculations were carried out for free amino acids, not residues incorporated into a peptide sequence. Moreover, Table 1 and Table S4 also demonstrate that the presence of these anchor residues is not always sufficient to guarantee surface contact at that point in the sequence. Specifically, Arg and His do not always act as contact residues; in contrast, Trp, Phe, Tyr, and Met *always* act as contact residues, regardless of where they appear in the sequence. These data indicate that for some anchors, the environment in which it is located can down-modulate its availability for making surface contact. Furthermore, these data show that while the presence of a large number of possible anchor residues in a sequence can confer a strong binding affinity (e.g., AuBP1), this is not always a necessary condition for the strongest binding (e.g., GBP1).

On the basis of previous calculations of amino acid binding strengths on the gold surface,<sup>68</sup> we have estimated the scale of the enthalpic contribution to the experimentally determined  $\Delta G$  values for each sequence by assigning a score to each contact residue in the sequence. These scores are then summed to provide a total enthalpic score for each peptide, which is then used to classify the binding enthalpy as Weak, Medium, or Strong for each sequence (see Supporting Information 'Contact Residue Scoring' for details). We have also estimated the scale of the conformational entropic contribution to  $\Delta G$  for each sequence. To accomplish this, we analyzed MD REST trajectories and characterized the ensemble of adsorbed configurations for each peptide sequence. We then used a clustering analysis (see Materials and Methods) to group together like structures (referred to as clusters herein) on the basis of similarity between backbone conformations. The number of distinct clusters for each adsorbed peptide is indicative of the number of different possible arrangements of the peptide in the adsorbed state, and is thus related to the conformational entropy of the adsorbed sequence. For example, a

sequence with a large number of distinct clusters, each with a relatively small population, is assigned high conformational entropy. Conversely, a sequence for which the top few clusters account for most of the population is assigned a low conformational entropy. The percentages of populations for the top 10 clusters for each adsorbed peptide are given in the Supporting Information, Table S5. Details of the classification of conformational entropy into low, medium, and high categories are also given in the Supporting Information (see 'Conformational Entropy Classification'). Finally, the conformational entropy classification for each adsorbed sequence is summarized in Table 1.

The range of experimental binding free energies in our sample of 12 peptides is rather narrow, with  $\Delta G$  varying by  $\sim 7$  kJ/mol across the entire set. The relatively small, yet important, differences in binding energies make discerning distinct sequence–structure–property differences among all of the peptides in the set challenging. In addition, taking into account the error bars on each binding free energy, we see the peptide affinities readily fall into two distinct binding regimes. On the basis of these two points, herein we will discuss in detail the most extreme cases for each of these two categories: the strongest binders (with the same binding free energy), AuBP1 and GBP1, and the weakest binder, Pd4. Before doing so, we comment on our findings for three other peptide sequences, starting with A3, for which there are previously reported simulation data.<sup>19</sup> In this previous MD simulation study, the adsorption energy of A3 at the aqueous Au(111) interface, calculated using the compartmentalized method, was  $-264$  kJ/mol, roughly 8 times the experimentally determined  $\Delta G_{\text{ads}}$  of  $-31.8$  kJ/mol reported here. Moreover, a very recent experimental study<sup>41</sup> indicates that A3 is capable of thermally activated surface diffusion at room temperature, once adsorbed onto gold; this seems unlikely if the binding energy was as great as  $-264$  kJ/mol. There are also some differences in the structural details reported by Heinz *et al.*<sup>19</sup> and our findings. These authors reported the A3 residues that were in direct contact with the surface. These authors reported direct contact for eight residues, A1–G5, P8, and P11–F12; the lack of Met anchoring is in contrast with the known strong attraction of sulfur-containing moieties for gold. In contrast, our REST simulations identified fewer anchors, with some anchor residues (Y2, G5, F12) in common with this previous study (see Table 1). We also found A6 and M8 as anchors. Further, our simulations indicate that no prolines served as anchor residues, not just for A3, but across all 12 peptides (contrast the entries for proline in Tables S4 and S5 in the Supporting Information).

Second, we compare our findings for AuBP2 against the recently published work of Corni *et al.*,<sup>32</sup> who used temperature-based REMD simulations of peptide adsorption at the aqueous Au(111) interface along with

the GoLP force-field.<sup>69</sup> These authors reported that the residues W1, R4, R5 and Y12, and to a lesser extent, R8 and R9, showed a reasonable probability (actual values not reported) of close contact with the gold surface. In comparison, we identify W1, R4, R5 and Y12 as anchor residues. Differences in the binding of R8 and R9 might be attributed to the use of the OPLS force-field<sup>70</sup> in GoLP, while we have used the CHARMM22\* force-field here. Similarly, we also compare our findings for QBP1 adsorption against those published by Corni *et al.*<sup>32</sup> These authors reported that W4, M8 and W11 spend the highest proportion of the trajectory in contact with the surface, and to a much lesser extent, so does Y7. In contrast, we find all four residues, W4, Y7, M8 and W11 as anchor residues; again, the difference could be attributed to differences between OPLS and CHARMM, particularly because of the high proline content of this sequence. However, crucially, both simulations identify Met as a strong-binding residue, in contrast to earlier simulations of Met-containing peptides such as A3<sup>19</sup> and GBP1.<sup>22,23</sup>

From Table 1, AuBP1 has five contact residues on average, four of which are anchors (one Trp and three Arg). The recent work of Corni *et al.* also identified these same four anchor residues.<sup>32</sup> Based on the classification, this provides a strong enthalpic contribution to the binding, which is combined with a medium entropic contribution. On the basis of this analysis, AuBP1 is therefore suggested to be an enthalpically driven binder. A typical configuration of the adsorbed state for AuBP1 is shown in Figure 3, revealing the overall close proximity of the entire peptide chain to the gold surface. This can be attributed to both the somewhat even spacing of the anchors along the peptide chain, and also the splayed Arg-Arg pair (R10-R11), providing additional lateral stability. The even spacing of the five contact residues along the chain ensures the peptide backbone cannot form loops that project away from the surface.

In contrast, GBP1, which has the same strong binding affinity, has fewer contact residues: three in total,

with two of these as anchors (one Met and one His). While our classification of the enthalpic contribution for GBP1 is medium, this sequence exhibits a high conformational entropy contribution (with the most extreme distribution of all the high entropy cases in our set of peptides: see Supporting Information, Table S6). We propose, therefore, that the moderate enthalpic component to the binding is enhanced by a substantial entropic term, thus motivating the classification of GBP1 as an entropically driven binder. Figure 4 shows representative conformations from the top two clusters for GBP1, revealing the C-terminal half of the peptide as being quite distant from the gold surface for both structures. This is due to the location of all three contact residues within the N-terminal region of the sequence, which ensures the peptide, up to residue position six, maintains close proximity to the gold surface. The remaining portion of the chain, from residue seven onward, is not pinned to the gold and thus experiences more conformational freedom compared to AuBP1. This is likely to be the source of the large entropic contribution to the binding affinity.

While no previously published modeling studies are available for the GBP1 peptide adsorbed onto gold, the adsorption onto gold of larger constructs of GBP1, such as the tandem triple repeat (3R-GBP1), has been modeled previously.<sup>22,23</sup> In contrast to our findings, these earlier studies identified the polar residues, serine and threonine, as the key residues that mediated contact with the surface. Moreover, both studies failed to identify methionine, a sulfur-containing residue, as a contact residue, again in contrast to our results. However, the large number of atoms in these tandem repeat systems implies that conformational sampling in both cases was far from optimal. Furthermore, recently published data for the adsorption of amino acids onto gold surfaces suggests threonine and serine do not have a strong affinity for gold.<sup>68</sup>

The relatively longer chain of GBP1 (14 residues), compared with other peptides in the set, is suggested to aid the entropic enhancement of the observed

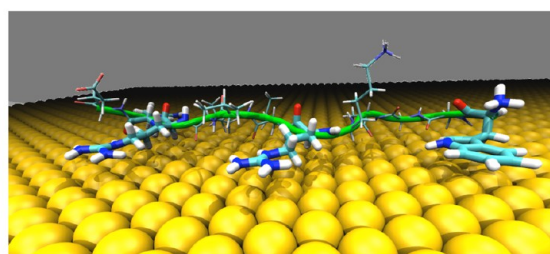
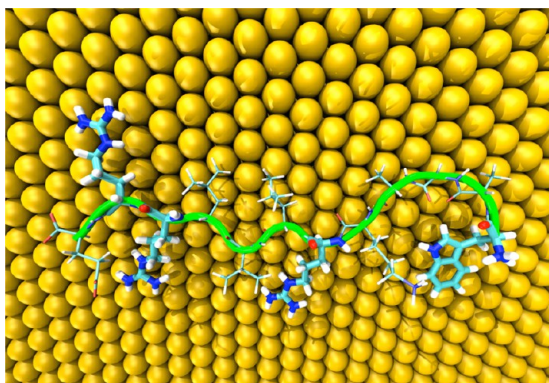


**Figure 3.** Typical structures (in both plan view and side view) for the surface adsorbed conformations of AuBP1. The anchor residues are highlighted with relatively thicker bonds. Waters are not shown for clarity.

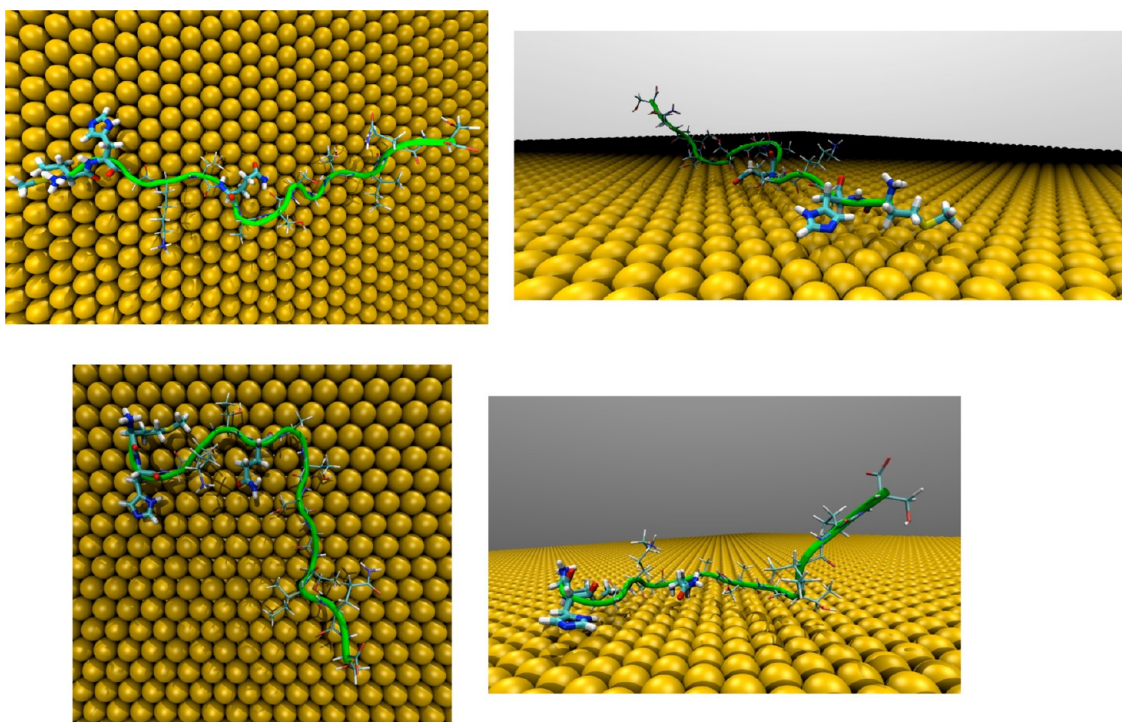


**Figure 4.** Typical structures (in both plan view and side view) for the top two clusters of the adsorbed conformations of GBP1 (top, cluster 1; bottom, cluster 2). In each case, the anchor residues are highlighted with relatively thicker bonds. Waters are not shown for clarity.

binding. Eight residues at the C-terminal region experience relatively greater conformational freedom, compared to the surface anchored residues at the N-terminal half of the chain. The uneven distribution of the contact residues in GBP1 is also predicted to positively impact the ability to successfully conjugate additional molecules to the surface-bound peptide, thus enabling the use of the sequence as a molecular tool to modify nanoparticle surfaces. Knowledge of the surface-bound peptide structure would allow for targeted regio-selective incorporation of functionalities on the nanoparticle surface, through peptide-surface patterning. In the case of GBP1, we predict that conjugation to the C-terminus, rather than the N-terminus will be least likely to adversely affect the gold-binding properties of the peptide; however, such a hypothesis would require both experimental and computational validation. This contrasts with AuBP1, where conjugation at either terminus could possibly down-modulate the availability of the anchor residues at positions 1 or 11. However, we note that for AuBP1 the lysine at position five is almost always found far from the surface, suggesting that conjugation to this residue may be a promising route for modification. Further, the lateral footprint of the adsorbed peptide is predicted to be smaller in the case of GBP1 compared with AuBP1. This difference may also impact the performance of peptides as nanoparticle ligands.

The weakest binder, Pd4, has only two contact residues on average, although both are anchor

residues (two His). Interestingly, this set of two anchor residues is in agreement with coarse-grained simulations of Pd4 adsorption on a palladium surface.<sup>20</sup> This leads to a classification of the binding enthalpy contribution as weak. On the other hand, the entropic contribution for this peptide is classified as high, although the population distribution for this sequence is not the most extreme case in the set (see Supporting Information, Table S6). We propose that, in contrast with GBP1, the very modest binding enthalpy has not been adequately offset by the entropic contribution, thus leading to a reduced binding affinity. Furthermore, the interval between these anchors in the sequence, and their location in the sequence, in positions 6 and 11, does not provide as much scope for conformational entropic contributions as compared to GBP1. This is because the Pd4 peptide chain cannot support high backbone mobility between the two anchor points, in addition to having a shorter, weakly bound, terminal domain (at the N-terminus, in contrast to the C-terminal domain in GBP1) relative to the case of GBP1. Interestingly, the average behavior of the anchor residues is not reflected in the top cluster in the adsorbed state. Specifically, the His at position eleven is not surface-bound in the top (most probable) cluster, while this residue is found to be in surface contact for most other clusters for this trajectory. These findings are illustrated in Figure 5, where we show the top two clusters for the surface-adsorbed Pd4 sequence.

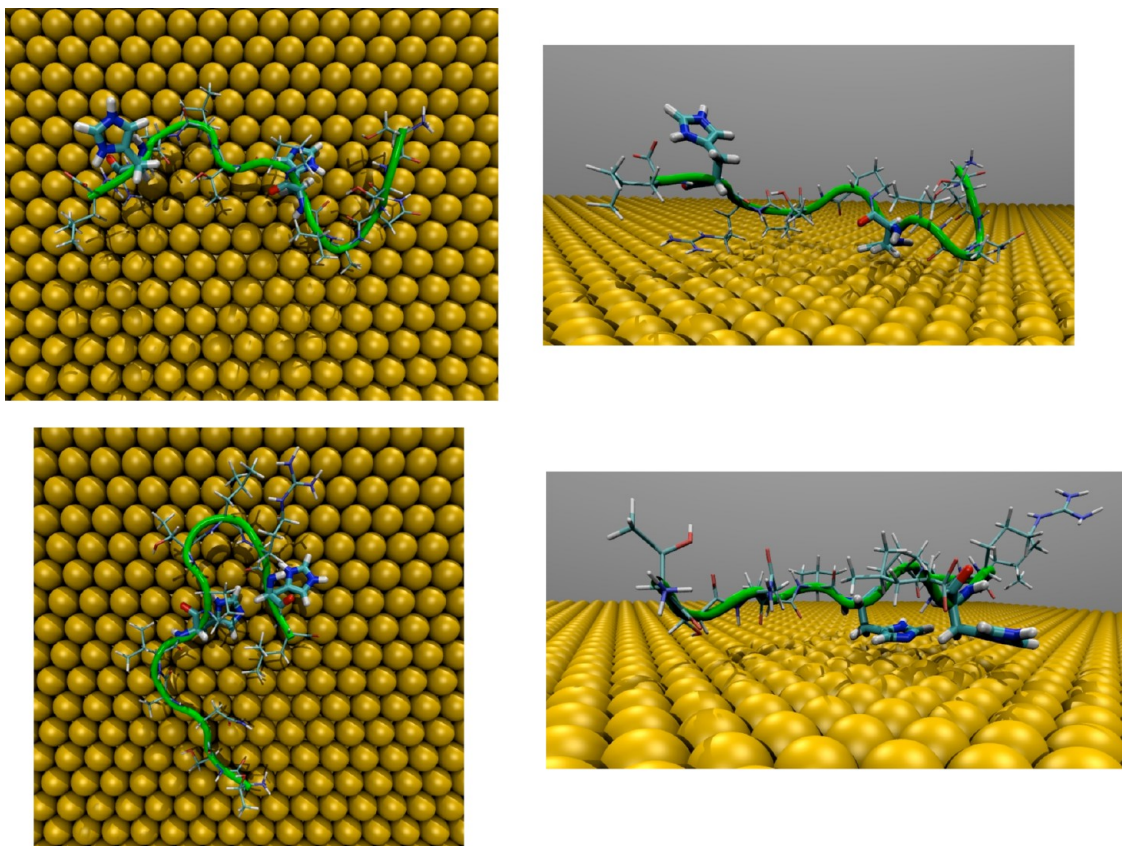


**Figure 5.** Typical structures (in both plan view and side view) for the top two clusters of the adsorbed conformations of Pd4 (top, cluster 1; bottom, cluster 2). In each case, the anchor residues are highlighted with relatively thicker bonds. Waters are not shown for clarity.

Taken together, the combination of the experimental and simulation results indicate that entropically driven peptide binding of nanoparticle surfaces is comparable to enthalpically driven binding. This contrasts with prior hypotheses that have focused solely on enthalpy-based interpretations of peptide–materials binding affinity. We suggest that one route to amplifying the conformational entropy contribution is to ensure the peptide has long and exposed unattached segments of the peptide chain when adsorbed at the surface. The high degree of freedom of the unattached region of the peptide chain can support many more configurational states compared with a sequence that is dominated by adsorbed conformations that are more fully pinned to the surface across the entire sequence.

## CONCLUSIONS

In conclusion, we have demonstrated that combined experimental and theoretical studies can reveal a fundamental basis for the affinity of peptides for target metallic nanosurfaces at the molecular level. These findings suggest that strong binding peptides can be broadly defined as either enthalpically driven, with a high number of anchor residues spaced evenly along the peptide chain, or entropically driven, with

fewer anchors spatially clustered at either end of the peptide chain. In the entropically driven case, one region of the peptide remains unbound, allowing for the large entropic contribution to dominate the binding thermodynamics. Such a hypothesis correlated well with the extremes of our set of experimentally observed  $\Delta G$  values. The absolute values of the binding energies of the peptides were also comparable to the well-known binding of thiols onto Au surfaces. For the peptides, however, multiple noncovalent interactions drive the binding process, in contrast to the single, nonspecific gold–sulfur bonding in thiol monolayers on gold. Thus, while their total binding affinities are high, the peptides are not irreversibly bound on the gold surface or to gold nanoparticles. This makes these peptides more amenable to nanoparticle surface modification for eventual applications, as compared to the covalently bound thiols. Furthermore, from the molecular modeling studies, anchor residues, as well as nonbinding sites, can be computationally predicted. This is useful information for designing peptide-based linker molecules for bionanocombintoric assembly of inorganic materials. Doing so requires chemical modification of the peptides to link them together *via* an additional biological or synthetic moiety. These modifications may change the peptide target binding

affinity, thus additional experimental and computational analyses of the altered peptide must be completed prior to assembly to understand such effects. The predictions of binding and nonbinding sites in the peptide sequence provide guidance on where attachment of a linker moiety is likely to have the smallest effect on binding. Interaction *via* multiple weak bonds, as in many biological systems, allows assemblies to evolve toward thermodynamic equilibrium states and reduces the possibility of kinetically trapping metastable configurations. At present our hypothesis of enthalpically and entropically driven

binders is capable of capturing only the broad features of the experimentally observed behavior; it does not take into account the subtle effects of the local environment around each anchor site and how this may down-modulate the availability of the anchor. These model refinements remain to be explored, as more gold-binding sequences become available. Moreover, the factors identified here can be incorporated into bioinformatics models that we are also developing. This provides guidance to such models based on the underlying molecular interactions.

## MATERIALS AND METHODS

**Chemicals.** All Fmoc-protected amino acids, Wang resins, and peptide synthesis reagents (piperidine (>99.0%), *N,N'*-diisopropylethylamine (DIPEA, >99.0%), *O*-(benzotriazol-1-yl)-*N,N,N',N'*-tetramethyluronium hexafluorophosphate (HBTU, >98.0%), and *N*-hydroxybenzotriazole monohydrate (HOBT hydrate, >98.0%)) were purchased from Advanced ChemTech. Trifluoroacetic acid (TFA, 99.5%) and triisopropylsilane (TIS, 98.0%) were purchased from Alfa Aesar. Ammonium hydroxide (20.0%) and hydrogen peroxide (30.0%) were purchased from VWR. Solvents including acetonitrile, methanol, and *N,N*-dimethylformamide for peptide synthesis and purification were purchased from VWR. All the chemicals were used as received. Nanopure water (18.2 MΩ·cm; Millipore, Bedford, MA) was employed for all experiments.

**Peptide Synthesis.** All of the peptides were prepared with a TETRAS model peptide synthesizer (Creosalus; Louisville, KY) employing standard Fmoc protocols.<sup>71</sup> After the synthesis was complete, the peptides were cleaved from the resins using a cleavage cocktail of 95% TFA, 2.5% TIS, and 2.5% water. The peptides were then purified *via* reverse phase HPLC with a 0.1% TFA aqueous solution and acetonitrile gradient. The peptides were finally confirmed by MALDI-TOF mass spectrometry.

**QCM Analysis.** QCM exploits the piezoelectric effect in quartz to measure changes in the resonant frequency of a quartz oscillator in response to an increase in mass due to molecular binding at the sensor surface.<sup>72,73</sup> This frequency change is directly related, *via* the Sauerbrey equation, to the mass of peptide adsorbed, from which binding kinetic parameters can be determined.<sup>46</sup> All QCM measurements, including those of dissipation energy, were completed using a Q-Sense E4 instrument (Biolin Scientific) employing standard gold crystal sensors. The oscillator frequency was recorded for 30.0 min to ensure that saturation of the frequency change was observed. The QCM sensors were first cleaned with a 1:1:5 (v/v/v) 30% H<sub>2</sub>O<sub>2</sub>/ammonium hydroxide/water solution for 5.0 min and then rinsed with copious amounts of water. The gold surface was dried with N<sub>2</sub> gas and subsequently subjected to UV/ozone cleaning prior to use. Once cleaned, the sensors were inserted into the QCM system, where the frequency change in pure water was recorded for ~5 min to determine chip integrity. Afterward, an aqueous peptide solution of a concentration between 2.5 and 15.0 μg/mL was flowed over the sensor surface, from which the frequency change and dissipation energy were recorded for ~30 min. All measurements were performed at 24.2 °C.

**SPR Analysis.** For surface plasmon resonance, a home-built system, based on measuring phase changes at the SPR coupling angle, was used.<sup>74</sup> A glass slide with a 50 nm thick gold coating was purchased from Platypus Technologies. A prism, with one face attached to the gold film using matching oil, and a flow chamber form a sensor head. First, water was flowed over the sensor head and a baseline was recorded. Afterward, an aqueous peptide solution of a concentration between 2.5 and 15.0 μg/mL was flowed in, from which the SPR phase change

was monitored until it reached a plateau. Water was flowed over the surface again to confirm the binding.

**Replica Exchange with Solvent Tempering (REST) MD Simulations.** A total of 12 REST<sup>24,25</sup> simulations were carried out, one for each peptide sequence listed in Table 1. All REST simulations reported here have modeled a single peptide chain (one each from our set of twelve sequences) adsorbed onto the planar Au(111) surface under aqueous conditions, using the Gromacs 4.5.5 software package.<sup>75</sup> Our recently developed polarizable GoLP-CHARMM force-field<sup>26</sup> was used here in partnership with the CHARMM22\*<sup>76,77</sup> and the modified TIP3P<sup>78,79</sup> force-fields. The REST simulations were implemented according to our recent development, testing and validation study,<sup>24,25</sup> in the *NVT* (Canonical) ensemble, with an effective temperature range spanning 300–433 K. A total of 16 replicas were used to span this effective temperature window. All REST simulations were carried out for 15 × 10<sup>6</sup> MD steps, yielding conformational sampling that is approximately equivalent to μs trajectories of conventional MD.<sup>24,80</sup> Additional details, including evidence of sampling efficacy (replica mobilities) and sampling equilibration, can be found in the Supporting Information (Methods C: Computational Details).

**REST MD Clustering Analysis.** Detailed analysis was carried out on the constant-ensemble run at an effective temperature of 300 K (herein referred to as the reference trajectory). We classified the Boltzmann-weighted ensemble from our reference trajectories into groups of like structures, on the basis of similarity of their backbone structures, *via* the Daura clustering algorithm with a root mean-squared deviation (RMSD) cutoff between backbone atoms of 2 Å. We performed our clustering analysis over the entire 15 ns trajectory in each case. The population of a given cluster was calculated as the percentage fraction of the number of frames that were assigned membership of that cluster, divided by the total number of frames in the trajectory.

**REST MD Contact Residue Analysis.** We define a contact residue as a residue that maintains persistent contact with the surface. To quantify persistent contact, first, for each reference trajectory, we calculated the distance between the topmost layer of the gold surface and each residue in the sequence. On the basis of these data, distance cut-offs were established to identify a range of separations where each particular residue was in immediate contact with the gold surface. We then calculated the fraction of frames in the reference trajectory for which each residue was found within the contact range of surface-residue separation. We then defined a residue to be a contact residue if that residue was found to bind persistently to the surface. Our definition of persistent contact was satisfied if the given residue was found within contact range for 65% of more of the last 5 ns of the reference trajectory. Further details including the data used to establish the cutoffs and further analysis based on variation of both the contact cutoff distance and the percentage of frames required to satisfy our definition of a contact residue are given in the Supporting Information (Methods D: MD Analysis).

*Conflict of Interest:* The authors declare no competing financial interest.

*Acknowledgment.* This material is based upon work supported by the Air Office of Scientific Research, Grant Number FA9550-12-1-0226. We gratefully acknowledge the Victorian Life Sciences Computation Facility (VLSCI) for allocation of computational resources. T.R.W. thanks **veski** for an Innovation Fellowship.

*Supporting Information Available:* Summary of peptide sequences and their target materials, summary of gold surface adsorption and desorption QCM data, film thickness calculations, frequency of occurrence of all possible residues in all 12 peptides, frequency of occurrence of contact residues, percentage population of the top-10 most populated clusters for each adsorbed peptide, SPR analysis details, typical structures of adsorbed peptides, computational methods for contact residue scoring and conformational entropy classification, water structuring comparison between GolP-CHARMM and CHARMM-METAL, comparison of adsorption energies and adsorption free energies for amino-acid adsorption calculated using GolP-CHARMM and CHARMM-METAL, comparison of conformational sampling approaches, example of growth of clusters with simulation time, example REST replica mobilities, MD analysis details, residue-surface separations, and summary of residue contact data. This material is available free of charge via the Internet at <http://pubs.acs.org>.

## REFERENCES AND NOTES

1. Daniel, M. C.; Astruc, D. Gold Nanoparticles: Assembly, Supramolecular Chemistry, Quantum-Size-Related Properties, and Applications Toward Biology, Catalysis, and Nanotechnology. *Chem. Rev.* **2004**, *104*, 293–346.
2. Sun, Y. G.; Xia, Y. N. Shape-Controlled Synthesis of Gold and Silver Nanoparticles. *Science* **2002**, *298*, 2176–2179.
3. Liu, S.; Chen, G. Y.; Prasad, P. N.; Swihart, M. T. Synthesis of Monodisperse Au, Ag, and Au-Ag Alloy Nanoparticles with Tunable Size and Surface Plasmon Resonance Frequency. *Chem. Mater.* **2011**, *23*, 4098–4101.
4. Yong, K. T.; Sahoo, Y.; Swihart, M. T.; Prasad, P. N. Growth of CdSe Quantum Rods and Multipods Seeded by Noble-Metal Nanoparticles. *Adv. Mater.* **2006**, *18*, 1978–1982.
5. Xia, Y.; Xiong, Y.; Lim, B.; Skrabalak, S. E. Shape-Controlled Synthesis of Metal Nanocrystals: Simple Chemistry Meets Complex Physics?. *Angew. Chem., Int. Ed.* **2009**, *48*, 60–103.
6. Kaur, P.; Maeda, Y.; Mutter, A. C.; Matsunaga, T.; Xu, Y.; Matsui, H. Three-Dimensional Directed Self-Assembly of Peptide Nanowires into Micrometer-Sized Crystalline Cubes with Nanoparticle Joints. *Angew. Chem., Int. Ed.* **2010**, *49*, 8375–8378.
7. Macfarlane, R. J.; Lee, B.; Jones, M. R.; Harris, N.; Schatz, G. C.; Mirkin, C. A. Nanoparticle Superlattice Engineering with DNA. *Science* **2011**, *334*, 204–208.
8. Hnilova, M.; So, C. R.; Oren, E. E.; Wilson, B. R.; Kacar, T.; Tamerler, C.; Sarikaya, M. Peptide-Directed Co-Assembly of Nanoprobes on Multimaterial Patterned Solid Surfaces. *Soft Matter* **2012**, *8*, 4327–4334.
9. Brown, S. Metal-Recognition by Repeating Polypeptides. *Nat. Biotechnol.* **1997**, *15*, 269–272.
10. Naik, R. R.; Stringer, S. J.; Agarwal, G.; Jones, S. E.; Stone, M. O. Biomimetic Synthesis and Patterning of Silver Nanoparticles. *Nat. Mater.* **2002**, *1*, 169–172.
11. Lu, Z. J.; Murray, K. S.; Vancleave, V.; Lavallie, E. R.; Stahl, M. L.; McCoy, J. M. Expression of Thioredoxin Random Peptide Libraries on the *Escherichia coli* Cell Surface as Functional Fusions to Flagellin: A System Designed For Exploring Protein-Protein Interactions. *Biotechnology* **1995**, *13*, 366–372.
12. Hnilova, M.; Oren, E. E.; Seker, U. O. S.; Wilson, B. R.; Collino, S.; Evans, J. S.; Tamerler, C.; Sarikaya, M. Effect of Molecular Conformations on the Adsorption Behavior of Gold-Binding Peptides. *Langmuir* **2008**, *24*, 12440–12445.
13. Whaley, S. R.; English, D. S.; Hu, E. L.; Barbara, P. F.; Belcher, A. M. Selection of Peptides with Semiconductor Binding Specificity for Directed Nanocrystal Assembly. *Nature* **2000**, *405*, 665–668.
14. Nam, K. T.; Kim, D. W.; Yoo, P. J.; Chiang, C. Y.; Meethong, N.; Hammond, P. T.; Chiang, Y. M.; Belcher, A. M. Virus-Enabled Synthesis and Assembly of Nanowires for Lithium Ion Battery Electrodes. *Science* **2006**, *312*, 885–888.
15. Brown, S.; Sarikaya, M.; Johnson, E. A Genetic Analysis of Crystal Growth. *J. Mol. Biol.* **2000**, *299*, 725–735.
16. Kim, J.; Rheem, Y.; Yoo, B.; Chong, Y.; Bozhilov, K. N.; Kim, D.; Sadowsky, M. J.; Hur, H.-G.; Myung, N. V. Peptide-Mediated Shape- and Size-Tunable Synthesis of Gold Nanostructures. *Acta Biomater.* **2010**, *6*, 2681–2689.
17. Slocik, J. M.; Stone, M. O.; Naik, R. R. Synthesis of Gold Nanoparticles Using Multifunctional Peptides. *Small* **2005**, *1*, 1048–1052.
18. Tamerler, C.; Oren, E. E.; Duman, M.; Venkatasubramanian, E.; Sarikaya, M. Adsorption Kinetics of an Engineered Gold Binding Peptide by Surface Plasmon Resonance Spectroscopy and a Quartz Crystal Microbalance. *Langmuir* **2006**, *22*, 7712–7718.
19. Heinz, H.; Farmer, B. L.; Pandey, R. B.; Slocik, J. M.; Patnaik, S. S.; Pachter, R.; Naik, R. R. Nature of Molecular Interactions of Peptides with Gold, Palladium, and Pd-Au Bimetal Surfaces in Aqueous Solution. *J. Am. Chem. Soc.* **2009**, *131*, 9704–9714.
20. Pandey, R. B.; Heinz, H.; Feng, J.; Farmer, B. L.; Slocik, J. M.; Drummy, L. F.; Naik, R. R. Adsorption of Peptides (A3, Flg, Pd2, Pd4) on Gold and Palladium Surfaces by a Coarse-Grained Monte Carlo Simulation. *Phys. Chem. Chem. Phys.* **2009**, *11*, 1989–2001.
21. Feng, J.; Slocik, J. M.; Sarikaya, M.; Naik, R. R.; Farmer, B. L.; Heinz, H. Influence of the Shape of Nanostructured Metal Surfaces on Adsorption of Single Peptide Molecules in Aqueous Solution. *Small* **2012**, *8*, 1049–1059.
22. Verde, A. V.; Acres, J. M.; Maranas, J. K. Investigating the Specificity of Peptide Adsorption on Gold Using Molecular Dynamics Simulations. *Biomacromolecules* **2009**, *10*, 2118–2128.
23. Braun, R.; Sarikaya, M.; Schulten, K. Genetically Engineered Gold-Binding Polypeptides: Structure Prediction and Molecular Dynamics. *J. Biomater. Sci., Polym. Ed.* **2002**, *13*, 747–757.
24. Wright, L. B.; Walsh, T. R. Efficient Conformational Sampling of Peptides Adsorbed onto Inorganic Surfaces: Insights from a Quartz Binding Peptide. *Phys. Chem. Chem. Phys.* **2013**, *15*, 4715–4726.
25. Terakawa, T.; Kameda, T.; Takada, S. On Easy Implementation of a Variant of the Replica Exchange with Solute Tempering in GROMACS. *J. Comput. Chem.* **2011**, *32*, 1228–1234.
26. Wright, L. B.; Rodger, P. M.; Corni, S.; Walsh, T. R. GolP-CHARMM: First-Principles Based Force Fields for the Interaction of Proteins with Au(111) and Au(100). *J. Chem. Theory Comput.* **2013**, *9*, 1616–1630.
27. Raut, V. P.; Agashe, M. A.; Stuart, S. J.; Latour, R. A. Molecular Dynamics Simulations of Peptide-Surface Interactions. *Langmuir* **2005**, *21*, 1629–1639.
28. Tomasio, S. D.; Walsh, T. R. Atomistic Modelling of the Interaction between Peptides and Carbon Nanotubes. *Mol. Phys.* **2007**, *105*, 221–229.
29. Tomasio, S. M.; Walsh, T. R. Modeling the Binding Affinity of Peptides for Graphitic Surfaces. Influences of Aromatic Content and Interfacial Shape. *J. Phys. Chem. C* **2009**, *113*, 8778–8785.
30. Skelton, A. A.; Liang, T. N.; Walsh, T. R. Interplay of Sequence, Conformation, and Binding at the Peptide-Titania Interface as Mediated by Water. *ACS Appl. Mater. Interfaces* **2009**, *1*, 1482–1491.
31. Oren, E. E.; Notman, R.; Kim, I. W.; Evans, J. S.; Walsh, T. R.; Samudrala, R.; Tamerler, C.; Sarikaya, M. Probing the Molecular Mechanisms of Quartz-Binding Peptides. *Langmuir* **2010**, *26*, 11003–11009.

32. Corni, S.; Hnilova, M.; Tamerler, C.; Sarikaya, M. Conformational Behavior of Genetically-Engineered Dodecapeptides as a Determinant of Binding Affinity for Gold. *J. Phys. Chem. C* **2013**, *117*, 16990–17003.

33. Wales, D. J. *Energy Landscapes*; Cambridge University Press: Cambridge, U.K., New York, 2003.

34. Hnilova, M.; Liu, X.; Yuca, E.; Jia, C.; Wilson, B.; Karatas, A. Y.; Gresswell, C.; Ohuchi, F.; Kitamura, K.; Tamerler, C. Multi-functional Protein-Enabled Patterning on Arrayed Ferroelectric Materials. *ACS Appl. Mater. Interfaces* **2012**, *4*, 1865–1871.

35. Oren, E. E.; Tamerler, C.; Sahin, D.; Hnilova, M.; Seker, U. O. S.; Sarikaya, M.; Samudrala, R. A Novel Knowledge-Based Approach to Design Inorganic-Binding Peptides. *Bioinformatics* **2007**, *23*, 2816–2822.

36. Pacardo, D. B.; Sethi, M.; Jones, S. E.; Naik, R. R.; Knecht, M. R. Biomimetic Synthesis of Pd Nanocatalysts for the Stille Coupling Reaction. *ACS Nano* **2009**, *3*, 1288–1296.

37. Wei, Y.; Latour, R. A. Determination of the Adsorption Free Energy for Peptide-Surface Interactions by SPR Spectroscopy. *Langmuir* **2008**, *24*, 6721–6729.

38. Wei, Y.; Latour, R. A. Benchmark Experimental Data Set and Assessment of Adsorption Free Energy for Peptide-Surface Interactions. *Langmuir* **2009**, *25*, 5637–5646.

39. Gerdon, A. E.; Wright, D. W.; Cliffel, D. E. Epitope Mapping of the Protective Antigen of *B. anthracis* by Using Nano-clusters Presenting Conformational Peptide Epitopes. *Angew. Chem., Int. Ed.* **2006**, *45*, 594–598.

40. Dickerson, M. T.; Abney, M. B.; Cameron, C. E.; Knecht, M.; Bachas, L. G.; Anderson, K. W. Fibronectin Binding to the *Treponema pallidum* Adhesin Protein Fragment rTp0483 on Functionalized Self-Assembled Monolayers. *Bioconjugate Chem.* **2012**, *23*, 184–195.

41. Nergiz, S. Z.; Slocik, J. M.; Naik, R. R.; Singamaneni, S. Surface Defect Sites Facilitate Fibrillation: An Insight Into Adsorption of Gold-Binding Peptides on Au(111). *Phys. Chem. Chem. Phys.* **2013**, *15*, 11629–11633.

42. So, C. R.; Tamerler, C.; Sarikaya, M. Adsorption, Diffusion, and Self-Assembly of an Engineered Gold-Binding Peptide on Au(111) Investigated by Atomic Force Microscopy. *Angew. Chem., Int. Ed.* **2009**, *48*, 5174–5177.

43. Love, J. C.; Estroff, L. A.; Kriebel, J. K.; Nuzzo, R. G.; Whitesides, G. M. Self-Assembled Monolayers of Thiolates on Metals as a Form of Nanotechnology. *Chem. Rev.* **2005**, *105*, 1103–1170.

44. Höök, F.; Kasemo, B.; Nylander, T.; Fant, C.; Sott, K.; Elwing, H. Variations in Coupled Water, Viscoelastic Properties, and Film Thickness of a Mefp-1 Protein Film During Adsorption and Cross-Linking: A Quartz Crystal Microbalance with Dissipation Monitoring, Ellipsometry, and Surface Plasmon Resonance Study. *Anal. Chem.* **2001**, *73*, 5796–5804.

45. Fischer, H.; Polikarpov, I.; Craievich, A. F. Average Protein Density is a Molecular-Weight-Dependent Function. *Protein Sci.* **2004**, *13*, 2825–2828.

46. Tamerler, C.; Duman, M.; Oren, E. E.; Gungormus, M.; Xiong, X.; Kacar, T.; Parviz, B. A.; Sarikaya, M. Materials Specificity and Directed Assembly of a Gold-Binding Peptide. *Small* **2006**, *2*, 1372–1378.

47. Seker, U. O. S.; Wilson, B.; Dincer, S.; Kim, I. W.; Oren, E. E.; Evans, J. S.; Tamerler, C.; Sarikaya, M. Adsorption Behavior of Linear and Cyclic Genetically Engineered Platinum Binding Peptides. *Langmuir* **2007**, *23*, 7895–7900.

48. Causa, F.; Della Moglie, R.; Iaccino, E.; Mimmi, S.; Marasco, D.; Scognamiglio, P. L.; Battista, E.; Palmieri, C.; Cosenza, C.; Sanguigno, L.; *et al.* Evolutionary Screening and Adsorption Behavior of Engineered M13 Bacteriophage and Derived Dodecapeptide for Selective Decoration of Gold Interfaces. *J. Colloid Interface Sci.* **2013**, *389*, 220–229.

49. Cohavi, O.; Reichmann, D.; Abramovich, R.; Tesler, A. B.; Bellapadrona, G.; Kokh, D. B.; Wade, R. C.; Vaskevich, A.; Rubinstein, I.; Schreiber, G. A Quantitative, Real-Time Assessment of Binding of Peptides and Proteins to Gold Surfaces. *Chem.—Eur. J.* **2011**, *17*, 1327–1336.

50. Sedlak, R. H.; Hnilova, M.; Grosh, C.; Fong, H.; Baneyx, F.; Schwartz, D.; Sarikaya, M.; Tamerler, C.; Traxler, B. Engineered *Escherichia coli* Silver-Binding Periplasmic Protein that Promotes Silver Tolerance. *Appl. Environ. Microbiol.* **2012**, *78*, 2289–2296.

51. Peele, B. R.; Krauland, E. M.; Wittrup, K. D.; Belcher, A. M. Design Criteria for Engineering Inorganic Material-Specific Peptides. *Langmuir* **2005**, *21*, 6929–6933.

52. Schnieder, J.; Colombi-Ciacchi, L. Specific Material Recognition by Small Peptides Mediated by the Interfacial Solvent Structure. *J. Am. Chem. Soc.* **2012**, *134*, 2407–2413.

53. Mijajlovic, M.; Penna, M. J.; Biggs, M. J. Free Energy of Adsorption for a Peptide at a Liquid/Solid Interface via Nonequilibrium Molecular Dynamics. *Langmuir* **2013**, *29*, 2919–2926.

54. Wang, F.; Stuart, S. J.; Latour, R. A. Calculation of Adsorption Free Energy for Solute-Surface Interactions Using Biased Replica-Exchange Molecular Dynamics. *Biointerphases* **2008**, *3*, 9–18.

55. Vellore, N. A.; Yancey, J. A.; Collier, G.; Latour, R. A. Assessment of the Transferability of a Protein Force Field for the Simulation of Peptide-Surface Interactions. *Langmuir* **2010**, *26*, 7396–7404.

56. Feng, J.; Pandey, R. B.; Berry, R. J.; Farmer, B. L.; Naik, R. R.; Heinz, H. Adsorption Mechanism of Single Amino Acid and Surfactant Molecules to Au {111} Surfaces in Aqueous Solution: Design Rules for Metal-Binding Molecules. *Soft Matter* **2011**, *7*, 2113–2120.

57. Heinz, H.; Lin, T. J.; Mishra, R. K.; Emami, F. S. Thermodynamically Consistent Force Fields for the Assembly of Inorganic, Organic, and Biological Nanostructures: The INTERFACE Force Field. *Langmuir* **2013**, *29*, 1754–1765.

58. Heinz, H.; Vaia, R. A.; Farmer, B. L.; Naik, R. R. Accurate Simulation of Surfaces and Interfaces of Face-Centered Cubic Metals Using 12–6 and 9–6 Lennard-Jones Potentials. *J. Phys. Chem. C* **2008**, *112*, 17281–17290.

59. Cerdá, J. R.; de Andres, P. L.; Flores, F.; Perez, R. Transport of Physisorbed Xe Atoms on Ni(110) Using a Scanning Tunnelling Microscope: A Theoretical Approach. *Phys. Rev. B* **1992**, *45*, 8721–8729.

60. Chen, D.-L.; Al-Saidi, W. A.; Johnson, J. K. The Role of van der Waals Interactions in the Adsorption of Noble Gases on Metal Surfaces. *J. Phys.: Condens. Matter* **2012**, *24*, 424211.

61. Bilic, A.; Reimers, J. R.; Hush, N. S. Adsorption of Pyridine on the Gold(111) Surface: Implications for “Alligator Clips” for Molecular Wires. *J. Phys. Chem. B* **2002**, *106*, 6740–6747.

62. Cicero, G.; Calzolari, A.; Corni, S.; Catellani, A. Anomalous Wetting Layer at the Au(111) Interface. *J. Phys. Chem. Lett.* **2011**, *2*, 2582–2586.

63. Wright, L. B.; Rodger, P. M.; Walsh, T. R.; Corni, S. First-principles Based Force-Field for the Interaction of Proteins with Au(100) (5 × 1): An Extension of GoLP-CHARMM. *J. Phys. Chem. C* **2013**, submitted for publication.

64. Willett, R. L.; Baldwin, K. W.; West, K. W.; Pfeiffer, L. N. Differential Adhesion of Amino Acids to Inorganic Surfaces. *Proc. Natl. Acad. Sci. U.S.A.* **2005**, *102*, 7817–7822.

65. Li, H.-Q.; Chen, A.; Roscoe, S. G.; Lipkowski, J. Electrochemical and FTIR Studies of Phenylalanine Adsorption at the Au(111) Electrode. *J. Electroanal. Chem.* **2001**, *500*, 299–310.

66. Barducci, A.; Bussi, G.; Parrinello, M. Well-Tempered Metadynamics: A Smoothly Converging and Tunable Free-Energy Method. *Phys. Rev. Lett.* **2008**, *100*, 020603.

67. Nadler, R.; Sanz, J. F. Effect of Dispersion Correction on the Au(111)-H<sub>2</sub>O Interface: A First-Principles Study. *J. Chem. Phys.* **2012**, *137*, 114709.

68. Hoefling, M.; Iori, F.; Corni, S.; Gottschalk, K.-E. Interaction of Amino Acids with the Au(111) Surface: Adsorption Free Energies from Molecular Dynamics Simulations. *Langmuir* **2010**, *26*, 8347–8351.

69. Iori, F.; Di Felice, R.; Molinari, E.; Corni, S. GoLP: An Atomistic Force-Field To Describe the Interaction of Proteins With Au(111) Surfaces in Water. *J. Comput. Chem.* **2009**, *30*, 1465–1476.

70. Kaminski, G.; Friesner, R. A.; Tirado-Rives, J.; Jorgensen, W. L. Evaluation and Reparametrization of the OPLS-AA Force Field for Proteins via Comparison with Accurate

Quantum Calculations on Peptides. *J. Phys. Chem. B* **2001**, *105*, 6474–6487.

- 71. Chan, W. C.; White, P. D. *Fmoc Solid Phase Peptide Synthesis: A Practical Approach*; Oxford University Press: New York, 2000.
- 72. Lu, C.; Czanderna, A. W. *Applications of Piezoelectric Quartz Crystal Microbalance*; Elsevier: New York, 1984.
- 73. O'Sullivan, C. K.; Guilbault, G. G. Commercial Quartz Crystal Microbalances—Theory and Applications. *Biosens. Bioelectron.* **1999**, *14*, 663–670.
- 74. Law, W. C.; Markowicz, P.; Yong, K. T.; Roy, I.; Baev, A.; Patkovsky, S.; Kabashin, A. V.; Ho, H. P.; Prasad, P. N. Wide Dynamic Range Phase-Sensitive Surface Plasmon Resonance Biosensor Based on Measuring the Modulation Harmonics. *Biosens. Bioelectron.* **2007**, *23*, 627–632.
- 75. Hess, B.; Kutzner, C.; van der Spoel, D.; Lindahl, E. Gromacs 4: Algorithms for Highly Efficient, Load-Balanced, and Scalable Molecular Simulation. *J. Chem. Theory Comput.* **2008**, *4*, 435–447.
- 76. MacKerell, A. D.; Bashford, D.; Bellott, M.; Dunbrack, R. L.; Evanseck, J. D.; Field, M. J.; Fischer, S.; Gao, J.; Guo, H.; Ha, S.; et al. All-Atom Empirical Potential for Molecular Modeling and Dynamics Studies of Proteins. *J. Phys. Chem. B* **1998**, *102*, 3586–3616.
- 77. Piana, S.; Lindorff-Larsen, K.; Shaw, D. E. How Robust Are Protein Folding Simulations with Respect to Force Field Parameterization? *Biophys. J.* **2011**, *100*, L47–L49.
- 78. Jorgensen, W. L.; Chandrasekhar, J.; Madura, J. D.; Impey, R. W.; Klein, M. L. Comparison of Simple Potential Functions for Simulating Liquid Water. *J. Chem. Phys.* **1983**, *79*, 926–935.
- 79. Neria, E.; Fischer, S.; Karplus, M. Simulation of Activation Free Energies in Molecular Systems. *J. Chem. Phys.* **1996**, *105*, 1902–1921.
- 80. Notman, R.; Oren, E. E.; Tamerler, C.; Sarikaya, M.; Samudrala, R.; Walsh, T. R. Solution Study of Engineered Quartz Binding Peptides Using Replica Exchange Molecular Dynamics. *Biomacromolecules* **2010**, *11*, 3266–3274.